# Performance of Third Generation Wave Models in Extreme Hurricanes

R. E. Jensen
USAE Waterways Experiment Station
Coastal Engineering Research Center
Vicksburg, MS


V. J. Cardone
Oceanweather Inc.
Cos Cob, CT


A. T. Cox
Oceanweather Inc.
Cos Cob, CT

## 1. INTRODUCTION

Numerical spectral wave prediction models based on third-generation (3G) source term physics have largely supplanted first and second generation models within the past decade in both real time and hindcast applications. The 3G models have been substantially validated in a wide range of extratropical wind forcing regimes (see e.g. Cardone et al., 1995 and Cardone et al., 1996) but only recently has their application to and performance in tropical cyclone cases been reported in the public domain (e.g. Cardone et al., 2004; Cox et al., 2005; Wright et al., 2001; Tolman et al. 2005). The two main obstacles to such studies have been the difficulty of specifying accurate surface wind fields in tropical cyclones and the scarcity of high-quality wave measurements in the inner high energy core of such systems.

This study takes advantage of significant advances made in recent years in the analysis of the time and space evolution of surface wind field in North Atlantic basin hurricanes made possible by new interactive kinematic reanalysis tools such as NOAA's HWnd (Powell et al, 1998) and OWI's IOKA based Tropical Analyst Workstation (Cox et al., 2002) and the exceptional (relative to data collected in tropical cyclone in other basins) wind data sets obtained by in-situ, airborne and satellite remote sensing systems. The integration of these various data sources and analysis systems into a NOPP supported operational coupled-model real time system for forecasting winds, waves and surge in land falling U.S. hurricanes is described recently by Graber et al. (2006).

The lack of measured wave data in the core of intense hurricanes has been relieved to some extent by the unprecedented occurrence of a number of Category 3, 4 and 5 hurricanes that have occurred since 2002 in the Gulf of Mexico (GOM), a basin with a fairly dense rich array of NOAA National Data Buoy Center (NDBC) moored data buoys. The most interesting datasets were collected in Hurricanes Lili (2002), Ivan (2004), Dennis (2005), Katrina (2005) and Rita (2005). These datasets join the previous high quality wave measurements in extreme Hurricane Camille (1969) acquired at an array of six offshore platforms in the industry sponsored Ocean Data Gathering Program (ODGP, Cardone et al., 1976). The peak significant wave height (Hmo) in the inner core of Camille, based on measurements, of about 14.5 meters is comparable to the 100-year estimated design Hmo for the north central GOM. NDBC buoys near the tracks of the recent storms recorded substantially higher sea states, including a peak Hmo of 16 m at buoy 42040 in Ivan and 16.9 m at the same buoy in Katrina (these are absolute reported peaks without consideration of uncertainty associated with sampling variability). Peak Hmo in excess of 10 m were were recorded at some buoys in Lili, Dennis and Rita. These buoy measurements provide a rare opportunity to evaluate the performance of modern 3G wave models in wave regimes far removed from those used for model tuning.

In this study, the performance of three variants of 3G wave model physics are evaluated by hindcasting Hurricanes Camille, Lili, Ivan, Dennis, Katrina and Rita. The models are WAM4.5, WAM4.5 with an upper limit applied to the ratio of friction velocity to wind speed (hence WAM4.5CAP) for the first time in this study, and OWI3G, a third-generation formulation, which over a decade ago had already incorporated the concept of a saturation of the drag coefficient at hurricane wind speeds. To isolate effects of model

physics, all models were adapted to the GOM on the same high resolution grid system, with the same bathymetry, employed comparable spectral resolution and were all driven by the same wind fields, which had been carefully reanalyzed following a kinematic approach to agree with the full suite of in-situ, aircraft and remotely sensed wind measurements acquired in the recent storms. The wind field of Camille was generated with a proven mesoscale dynamical model initialized with a revised set of inputs.

This paper gives a preliminary evaluation of the hindcasts. A more in-depth analysis and interpretation of the results will be presented in a journal paper in preparation. The alternative hindcasts were evaluated against time series of Hmo and dominant wave period (Tp) and (if available) direction at all deep-water buoys within about 100 nm of the respective storm tracks but only a sample of that analysis is presented in this paper, which focuses mainly on the hindcast of peak sea states in the storm inner core along the storm track and at the buoy sites considered. Perhaps not surprisingly, these hindcasts exhibited larger variance in specification of peak storm HS than exhibited by contemporary 2G and 3G wave models in extra-tropical storm regimes. In addition, whereas most contemporary wave models tend to underestimate peak sea states in the most severe extra-tropical cyclones, the current standard WAM variants (cycles 4 and 4.5) tends to overestimate peak HS in the most severe tropical cyclones. The variants in which the surface drag coefficient is effectively capped above wind speeds of about 30 m/s, out performed the formulation in which the drag was allowed to float according to the wave induced drag formulation of Janssen (1991). This result is consistent with recently reported direct measurements of the drag coefficient at hurricane wind speeds (Powell et al., 2003) and with recently reported numerical experiments carried out with a wave boundary layer model (Moon et al. 2004).

## 2. HURRICANE WIND FIELD SPECIFICATION

Figure 1 show the tracks of the six GOM hurricanes modeled and also the locations of the NDBC moored buoys that acquired wave measurements in one or more of the five 21st century storms.

The wind fields used for the present hindcast were developed by an analysis method that has been applied with more or less complexity depending on available data, in over three-dozen studies involving almost all basins on the globe within which tropical cyclones can occur. The method starts from raw data

whenever possible and includes an intensive reanalysis of traditional cyclone parameters such as track and intensity (in terms of eye minimum pressure) and then develops new estimates of the more difficult storm parameters, such as the properties of the radial pressure profile associated with the symmetric part of the cyclone as follows:

Po       minimum central pressure
Pfar    far-field pressure
Rp      scale radius of exponential pressure profile
B        profile peakedness parameter

B is an additional scaling parameter introduced by Graham and Hudson (1960) whose significance was discussed by Holland (1980).

The time histories of all of these parameters are specified within the entire period to be hindcast. Storm track and storm parameters are first used to drive a numerical primitive equation model of the cyclone planetary boundary layer (PBL) to generate a complete picture of the time-varying wind field associated with the cyclone circulation itself. That solution is then compared to time histories of accurately measured surface winds (reduced to standard height) at available measurement sites, and if necessary the storm parameters are varied and the model iterated until good agreement is obtained between the modeled wind field and the discrete high-quality wind observations available. Based on as yet unreported studies, we have found that wind speeds reported by NDBC 3-meter discus buoys are biased low in high wind speeds (> 30 m/s) and high sea states, say Hmo > 5 m (see also Gilhousen et al, 2006), even after the continuous 10-minute winds are averaged to 30-minute means and raised to 10-meter elevation. As a result we adjust the NDBC 3-meter discus buoy wind speeds with an in-house sea state dependent algorithm before using them. Wind speeds from NDBC NOMAD hull buoys are similarly affected but to a lesser extent (there are currently no NOMAD hulled buoys in GOM) while winds from the older 10-meter and 12-meter discus buoys appear to be unbiased at hurricane speeds.

An additional data source available in the GOM in recent years (since about 1998) is provided by the NOAA HRD HWnd snapshots, which focus on the inner core wind structure. In general, the PBL and HWnd approaches may be viewed as complementary so when both are available, the PBL solutions and the HWnd solutions are blended using OWI's IOKA (Interactive Objective Kinematic Analysis) system to

impose even higher accuracy and time continuity to the wind field than provided by either source alone. This resulting inner core tropical wind field is then blended into a basin-wide field, which incorporates both atmospheric modeled winds, in-situ measurements from buoys, CMAN stations, ship reports as well as satellite estimates of wind from altimeter and scatterometer instruments. The process is described in more detail in Cox and Cardone (2000) and was applied to all storms studied here except for Camille, whose wind field was modeled exclusively with the PBL model. The HWnd system is described by Powell et al. (1998). The PBL model (TC96) is described by Thompson and Cardone (1996). Comparisons of modeled wind fields with over-water measurements from buoys and rigs support an accuracy specification of ± 20 degrees in direction and ± 2 meters/second in wind speed (30-minute average at 10-meter elevation). Many comparisons have been published (see e.g., Ross and Cardone, 1978; Cardone and Ross, 1979; Forristall *et al.*, 1977; 1978; Forristall 1980; Cardone *et al.*, 1992, Cardone and Grant, 1994).

For the 21st century GOM hurricanes, there is a rich database typically available for consideration as outlined below:

- Aircraft reconnaissance data obtained from NOAA and U.S. Air Force hurricane hunter aircraft, including vortex messages as well as continuous flight level wind speed, direction, D-Value, air temperature.
- Gridded and image fields of marine surface wind composites from the Hurricane Research Division HWnd re-analysis
- Synoptic observations from NOAA buoy and C-MAN stations
- Synoptic observations from coastal and land stations obtained from the GTS (Global Transmission System) in real time
- NOAA NHC/TPC advisories including intensity and position at 3-hourly intervals.
- NHC/TPC best track data
- NHC/TPC Tropical Storm Report
- Composite NWS radar imagery
- Loops of NOAA GOES visual, infared and water vapor imagery
- NWS synoptic weather analysis charts
- NCEP model wind fields
- QUIKSCAT scatterometer winds
- TOPEX altimeter winds and waves
- ERS-2 altimeter winds and waves

- Aircraft tail radar Doppler wind speed images(Katrina only)
- Passive microwave images from the satellite mounted instruments AMSR-E,TRMM and SSMI

Figure 2 compares the wind fields for the six storms in terms of the envelope of the maximum wind speed specified over the whole grid domain. This plot demonstrates the remarkably wide range of sizes and shapes that intense Gulf hurricanes may exhibit. Camille was a very tight Category 5 storm with radius of maximum wind speed of only 10 Nm and maximum inner core wind speed of 56 m/s. There is very little along-track variation in the wind field shape and intensity, partly because aircraft reconnaissance was much less frequent, though the available once daily penetrations strongly support the notion that Camille was in nearly steady state and at Category 5 intensity during the 36-hour pre-landfall period. The wind fields of Lili and Dennis are also of the Camille-like "narrow" type but of lower inner core intensity with peak modeled wind speed of 48 m/s in Lili and 41 m/s in Dennis. Unlike Camille, both of these storms exhibited a pre-landfall (i.e. within about 90 nm of the coast) weakening, which appears to be a property of most well observed central Gulf intense hurricanes (Cooper et al, 2005). On the other hand, the wind fields of Ivan, Katrina and Rita were of much larger spatial scale than Camille, Lili and Dennis and exhibited considerable along-track variability in the inner core wind strength. Peak analyzed wind speeds were 58 m/s, 57 m/s, and 58 m/s in Ivan, Katrina and Rita respectively. All of these storms reached Saffir-Simpson Scale Category 5 intensity but in different places. Ivan attained peak intensity as its center passed western tip of Cuba while Katrina and Rita attained peak intensity in the area well south of the Mississippi delta in the general region occupied by the Loop Current. These storms were also of considerably lower intensity at landfall. Excellent accounts of the meteorological history of each of the storms modeled here may be found at the web site of the NOAA Tropical Prediction Center (TPC) at http://www.nhc.noaa.gov/pastall.shtml

## 3. WAVE MODELS

Figure 3 shows the grid system and bathymetry common to the alternative wave models run in this study. The basin grid is of spacing .05 degrees in latitude and longitude. Bathymetry is specified from

the GEBCO centenary 1-minute dataset. Shallow water effects are included on the basin grid with static water depth.

## 3.1 WAM4.5

The evolution of third generation wave modeling technologies was spawned from the SWAMP (SWAMP Group 1985) where a series of inter-comparisons were made on academic tests for state-of-the-art 2nd Generation wave models. Over the next 10-years the model called WAM (WAMDIG, 1988, Komen et al, 1994) has evolved from Cycles 1 through its last official release Cycle 4.0. in 1992 (Gunther et al 1992). Over this evolutionary process the greatest change in WAM was the incorporation of the *quasi-linear coupling* of the air-sea boundary described by Jannsen, (1991). In general, this mechanism accounted for the increased roughness length for spatial wind-wave growth processes. The reasoning was to counteract the tendency of WAM to under estimate wave heights for conditions greater than about 9-m. The atmospheric input source term was also modified from a Snyder et al. (1981) to a more basic Miles-Phillips mechanism. The dissipation source term was changed to properly estimate growth characteristics and source term balance. Other versions of WAM have been distributed, for example WAM Cycle 5 (Hersbach, and Janssen, 1999), and the European Centre for Medium Range Weather Forecast version of WAM described in Bidlot et al., 2005.

The version of WAM used in this study is been appropriately called Cycle 4.5. This version differs from all other of the WAM cycles in that 4.5 has incorporated improved numerical stability requirements for shallow water implementation; removed the dependency on source term time stepping to be equal to the propagation time step; improved the *limiter* requirements for the source term integration; and added depth-limited wave breaking. In addition to these major changes the architecture of the source code has been modified from FORTRAN 77 to FORTRAN 90, and using a suite of modules.

WAM 4.5 like its counterparts solves the action balance equation for the time rate change of directional wave spectra over a fixed grid.

$$\frac{DN(\vec{x},t,f,\theta)}{Dt} = \sum_i S_i$$

(1)

where $N(\vec{x},t,f,\theta)$ is the wave action and equal to $E(\vec{x},t,f,\theta)/\omega$ where E is the directional wave spectrum in frequency (f) and direction ($\theta$), and $\omega$ is the radial frequency. $S_i$ represents the source sink mechanisms:

$$\sum_i S_i = S_{in} + S_{nl} + S_{ds} + S_{w-b} + S_b$$

(2)

and $S_{in}$ is the atmospheric source term, $S_{nl}$ is the nonlinear wave-wave interaction, $S_{ds}$ is the high frequency dissipation, $S_{w-b}$ is the sink mechanism for bottom effects and $S_b$ is the sink mechanism for depth limited wave breaking.

The action balance equation is solved in two steps. The first is to solve for the spatial change in action density, or the second term on the right hand side of the equation below:

$$\frac{DN(\vec{x},t,f,\theta)}{Dt} = \left\{ \frac{\partial}{\partial t} + \vec{c}_g \cdot \frac{\partial}{\partial \vec{x}} \right\} N(\vec{x},t,f,\theta)$$

(3)

where $\vec{c}_g$ is the group speed of the wave component defined at each frequency and is functionally related to the water depth based on the linear dispersion:

$$\omega^2 = g \kappa \tanh(\kappa h)$$

(4)

and $\omega$ is the radial frequency ($\omega=2\pi f$), h is the water depth and $\kappa$ is the wave number ($\kappa=2\pi/L$, where L is the wavelength defined at frequency f, and dependent on the water depth).

The advection (propagation) and source term integration numerical scheme adopts a first-order upwind configuration. This requires less computational time, however does create the potential for *garden-sprinkler* effects (Tolman, 2002). Solution to Equation (3) is numerically solved in two parts. Advection of action is solved first or that found in the second term of the bracketed expression in Equation (3). Once the spectra are updated from propagation over the fixed grid, the source term integration is computed or $\partial N/\partial t$. The computational burden on this step is generally an order of magnitude greater than the propagation step, where the source term time step is set to assure a

consistency between the relaxation time of the processes to that of the numerical integration.

## 3.2 OWI3G

Computational details on the OWI's 3rd generation physics can be found in Khandekar *et al*. (1994) and Forristall and Greenwood (1998). OWI3G follows rather faithfully the formulation of the first 3G spectral wave model, WAM (WAMDI, 1988) with a few notable exceptions as noted below.

*The Spectral Resolution*

Direction: 24 bands. Band 1 is centered 7.5° clockwise from true north, the width of each band is 15°

Frequency: Band 1 is centered on 0.039 hz; the bands increase in geometric progression (ratio = 1.10064) to band 23, .32157 hz. This binning is negligibly coarser than used WAMDI (ratio = 1.100) and no coarser than that used in typical 15 frequency binning of ODGP.

*Propagation Scheme*

The downstream interpolation scheme described by Greenwood et al. (1985) is used throughout. Propagation over a time step at a grid point is implemented within the alternate growth-propagation cycle in the model integration by forming linear combinations of spectral variances at neighboring points. The weights used are extracted from a pre-computed table of propagation coefficients, which vary by latitude only in deep water, and are specific to each grid point in shallow water. The table of interpolation coefficients is calculated based upon great circle wave ray paths in deep water; in shallow water the weights are calculated following a ray tracing study through a digital bathymetry resolved on the wave model grid.

The limiting water depth for shallow propagation and growth processes is taken according to the conventional definition:

$kd > \pi$ , where $k = .006123$ m$^{-1}$ for the .039 Hz frequency bin.

*Spectral Growth/Dissipation Algorithms*

The spectral growth algorithm used in OWI3G follows closely that of WAM. OWI3G combines a source term representation and integration scheme based upon WAM with the propagation scheme described above. The source terms follows the theoretical forms used in WAM but with different numerics and code and with the following modifications. First, a linear excitation source term is added to atmospheric input terms, $S_{in}$, taken as a downscaled variant of the term used in OWI's 1G ODGP model (see e.g. Khandakar et al., 1994 for a description of the 1G model source terms). This allows the sea to grow from a flat calm initial condition in OWI3G, unlike all cycles of WAM which require an artificial warm start from a prescribed initial spectrum. The exponential input term is the empirical form of Snyder et al. (1981) with a slightly rescaled coefficient, in which $S_{in}$ is taken as a linear function of friction velocity $U_*$. However, unlike WAM in which $U_*$ is computed from the 10 meter wind speed $U_{10}$ following the drag law of Wu (1982), in OWI3G, a different drag law is used that was developed in the model tuning stage. That drag law follows Wu closely up to about 20 m/sec then becomes asymptotic to a constant at wind speeds above 30 m/s. It appears that OWI3G was the first wave model to incorporate a saturation surface drag formulation. That is, rather than retain the usual unlimited linear increase of the drag coefficient with increasing wind speed, OWI3G capped the drag coefficient at a value of 2.2 x 10$^{-3}$ which is reached at a wind speed of 29.5 m/s. Recent estimates of the 10-m surface marine drag coefficient in extreme winds in the field (Powell et al., 2003) and in a wind-tunnel/wave-tank set up (Donelan et al., 2005) tend to support the notion of saturation of the drag coefficient at high wind speeds.

The non-linear term is approximated by the standard DIA except that in OWI's model a second quartet of interactions is included as described by Forristall and Greenwood (1998). As in WAM, the non-linear transfer for waves in shallow water are described by the deep water transfer multiplied by a scaling factor which is a function of wave number and water depth (see Hasselman and Hasselman, 1985).

The dissipation source term, $S_{ds}$ is also taken from WAM except that the dependence on frequency is cubic rather than quadratic.

OWI3G was developed based upon tuning runs against the fetch-limited growth benchmark for 20 m/s wind speeds under constant winds used to tune

WAM, and trial hindcasts of a well-documented moderate extratropical cyclone (SWADE IOP-1, see Cardone et al., 1995) and two intense Gulf of Mexico hurricanes (Camille, 1969; Frederick, 1979). The bottom friction source term is a simple quadratic law with a specified tunable friction factor. OWI3G uses the same friction factor found in the North Sea version of WAM (NEDWAM) to yield skillful shallow water predictions. That factor, .076, is exactly twice the value originally proposed for WAM, which was based upon studies of pure swell attenuation in the North Sea JONSWAP experiment.

An interesting comparison of the performance of OWI's first generation (1G) model and and OWI3G in an extratropical setting is given by Khandekar, et al. (1994) A comparison of the performance of OWI1G, OWI3G and the latest cycle of WAM (WAM-4) in extreme storms is given in Cardone et al. (1996). Much more extensive validations of OWI's 3G wave model in long-term hindcast studies are given recently by Swail and Cox (2000) and Cox and Swail (2001) and Swail et al.( 2006).

### 3.3 WAM4.5CAP

The application of WAM4.5 in the first experimental version of the NOPP real time system noted above suggested as early as the 2004 season, in storms such as in the very small Hurricane Charlie and very large Hurricane Ivan, that peak Hmo in the inner core of hurricanes was biased high significantly. These storms were characterized by peak wind speeds of Category 4 and 5 level, and given the new evidence on the behavior of C10 at such wind speeds reported by Powell et al. (2003) and Donelan et al. (2005), the C10 implied by the wind stress calculates within WAM4.5 was examined. Figure 4 is an example of what was found. This plot gives the effective C10 carried by the WAM4.5 atmospheric input algorithm (see Janssen , 1991) computed as follows from standard model output

$$C10 \ = \ (U*/U10)**2$$

Where U* is friction velocity and U10 is effective neutral wind speed at 10-meter elevation. The plot also shows C10 consistent with a standard Charnock roughness formulation

$$Z0 \ = Ag* U**2/g$$

with a Charnock constant, Ag, of .015.

As expected the Charnock drag law seems to serve as an effective floor of C10, but clearly the wave induced drag contribution leads to very high values of C10 beginning at wind speeds of about 15 m/s and at hurricane wind speeds C10 ranges as high as 8 x 10-3. Almost all of the values of C10 above say 4 x 10-3 are associated with high sea states and hurricane wind speeds (incidentally, the official threshold wind speed for hurricane intensity is a peak 1-minute average wind speed greater than 64 knots which transforms to a 30-minute average wind speed of 28 m/s), a region in which, according to Powell et al and Donelan et al, C10 is effectively capped below a value of about 3 x 10-3 and may in fact even decrease at wind speeds greater than 40 m/s..

The simplest way to incorporate the concept of a saturation drag coefficient in WAM4.5 in hurricane regimes without disturbing the model behavior at wind speeds of 20 m/s and below is to cap the computed ratio

$$CAP \ = Max \ (U*/U10)$$

before the atmospheric input source term is computed. The optimum value of CAP was explored in evaluation of a number of trial hindcasts of well documented Camille against the peak Hmo measured at the ODGP array (see Figure 1 for locations of the stations in this array). Figure 5 shows the comparison of the hindcasts and measurements for CAP ranging from .05 to .06. Clearly, the nominal model is biased high and the run with CAP = .05 is biased low at the stations nearest the storm track. CAP = .06 was selected for the runs to be made on the 21st century storms reported here. This yields a cap on C10 of 3.6 x 10-3, which is still greater than the reported field experiments and the cap in OIW3G but this is a natural consequence of application of the CAP to the nominal WAM4.5 combination of atmospheric input and dissipation source terms of WAM4.5, which were tuned to provide a good source term balance together with the wave drag formulation, and which appears to work well in most extratropical and non—extreme-hurricane wave regimes. In those regimes, nominal C10 rarely ventures above 3.6 x 10-3.

### 4. VALIDATION

Validation of the wind and wave hindcasts of the 21st century hurricanes was performed against NDBC buoys in the GOM moored in deep water and sufficiently close to the tracks of the storms to record

Hmo peaks of at least 3 meters. Data were obtained from quality controlled files available from the National Oceanographic Data Center and have undergone additional quality control procedure not possible in real-time. The Hmo data are smoothed +/- 1 hour with equal weighting to reduce sampling variability. Figure 1 shows the locations of the buoys with respect to the storm tracks.

*Time History Comparison*

Figure 6 gives an example of a time history comparison, in this case at buoy 42001 in Lili. The path of Lili passed very close to NDBC buoys 42001 which is a 10-meter discus buoy with wind measurements at 10 meters above the sea surface. 42001 reported an 11.2-meter peak significant wave height at 02/21 GMT with adjusted wind speed of 47.2 m/s one hour later (both unsmoothed). As the east side of the eye wall passed 42001, Lili was at its maximum intensity as a Category 4 hurricane with minimum eye pressure of 938 mb. An Air Force plane at 700 mb measured flight level wind speeds of 142 knots, which reduce to 10-meter sustained winds of 128 knots using the most recent reduction factors. This intensity appears to be confirmed by GPS dropwindsonde measurements of near-surface wind speed of up to 123 knots at the time. The buoy recorded a peak gust of 130 knots, the highest wind speed ever recorded by a NOAA NDBC buoy. Note that all three wave models produced a good simulation of the overall time history of peak Hmo, associated peak spectral period and mean wave direction (see Cardone et al., 2004 for a more detailed comparison of the OWI3G hindcast and buoy data including comparisons of 2D wave spectra). However, WAM4.5 overestimated the peak Hmo by nearly 30% while WAM4.5CAP and OWI3G are within about 10% of the buoy peak.

*Absolute Storm Peaks*

Table 1 gives the absolute storm peak Hmo specified by each model in the basin and Figure 7 shows the same data in terms of a histogram. In Camille, Ivan Rita and Katrina, WAM4.5 yielded peak Hmo between 20 m and 25 m in each storm. While it is not possible to absolutely verify that these wave heights did not occur in any of these storms, there is convincing evidence in the ODGP Station 1 data that Hmo did not exceed 15 m Camille, and in platform damage analyses and several inversely modeled (estimates of peak wave heights from floating platforms at which motion were recorded (see e.g.

Leverette et al., 2005) that peak Hmo did not exceed 18 m in Ivan or Katrina. There is direct evidence in the Lili impact at buoy 42001, that the peak Hmo in Lili did not exceed 12m where WAM 4.5 gives 14 m. WAM4.5CAP provides peak Hmo over the six hurricanes modeled that is on average 23% lower then WAM4.5 while OWI3G provides peaks that are on average 28% lower than WAM4.5 and therefore 5 % lower than WAM4.5CAP. The bias appears to be independent of storm size. Figure 8 compares plots of the envelope of peak Hmo in very tight Camille and very large Katrina. This is, of course, explained by the control of absolute wind speed on the drag cap, rather than, say, storm size, fetch or wave age.

*Model versus Buoy Storm Peak Hmo and TP*

In this section we present evidence that the relative model differences in the specification of absolute storm peak Hmo and associated TP are also exhibited when the individual model hindcasts are compared to the buoy data in the 21st century hurricanes. The comparisons are limited to buoys moored in relatively deep water (water depth greater than 50 m) to avoid consideration of additional issues that may be associated with shallow water source terms, and to buoys which reported peak Hmo of at least 3 m in order to eliminate cases where peaks were associated with storm peripheral wind fields or mainly propagated swell. Table 2 gives the 26 available comparisons. The smoothed buoy Hmo peaks range from 3 m to 15.7 m. WAM4.5 yields a range of 2.5 m to 19.5 m., WAM4.5CAP yields a range of 2.5 m 16.0 m and OWI3G yields a range of peaks from 2.4 m to 14.4 m. The comparisons are presented as scatter plots for Hmo and associated TP in Figures 9 (WAM4.5), 10 (WAM4.5CAP) and Figure 11 (OWI3G). The statistics of the paired differences are given in Table 3.

WAM4.5 yields excellent skill up to about Hmo of 8 m but the hindcasts becomes increasingly positively biased at higher sea states. The mean difference in Hmo is +.89 m with scatter index of 0.24 which is higher than the threshold of 0.15 generally considered to be upper threshold of good skill. WAM4.5 also exhibits a pervasive positive bias in TP suggesting that over specification of peak period near the track of inner core sea states is contaminating much of the inner core. It is well known that in a hurricane environment the directional spectrum is quite complicated as wave energy generated in one quadrant of the storm propagates radially away from

the center and mixes with locally generated winds in other quadrants.

WAM4.5CAP dramatically improves the hindcasts at the buoys. The positive bias in Hmo is eliminated and the scatter index, at 0.17 is now much closer to 0.15. The period bias and scatter is reduced but still rather large. The bias in the OWI3G hindcasts is +0.03m and scatter index is 0.14. TP is biased low by 0.72 s but skill is excellent as shown on the scatter plots and the correlation coefficient of 0.95. These comparisons clearly show that the two model variants with capped drag (WAM4.5CAP and OWI3G) clearly outperform the nominal WAM variant. OWI3G outperformed WAM4.5CAP but perhaps this should be expected since its WAM Cycle3-type source term formulation was frozen in 1994 after a tuning process that involved the hindcast of two GOM hurricanes (Camille and Frederic).

## 5. DISCUSSION

This paper highlights the need for a more comprehensive formulation of the atmospheric input source term than included in current cycles of WAM. The formulation needs to take into full account the interaction of the atmospheric surface boundary layer model with a wavy surface that is under the influence of extreme wind speeds, such as intense tropical cyclones and even the most intense extratropical storms, recently dubbed "winter hurricanes" (see. e.g Von Ahn et al., 2006). Such a formulation presumably needs to consider the effects on the air-sea momentum flux associated with processes such as extensive white water coverage, foam generation, and spray production and transport. Janssen (1991) was the first to account for the wave induced contribution to wind stress within a wave model on the assumption that the wind input term of WAM may be taken to account for the interaction of the SBL and the wave surface across the entire spectrum. This mechanism, however, appears to greatly overestimate wind stress as a function of wave age at high wind speeds and at least in hurricane regimes. Powell et al. (2003) speculate that the wind stress is limited in the inner core of hurricanes by the extensive white water coverage of the waves. Bye and Jenkins (2006) argue that the reduction of drag at high wind speeds is primarily a consequence of spray production and a resulting thick and fast moving spray layer within the SBL, which not only reduce the drag coefficient but may also serve to transfer energy to longer wavelengths and thereby "flatten" the sea surface. Moon et al. (2004) have incorporated a coupled wave surface-SBL into the WW3 model and report some promising preliminary results.

Until an improved atmospheric input source treatment is incorporated into WAM4.5 we recommend capping the drag coefficient as was applied in this study. The adoption of a universal wind speed dependent cap is admittedly a simplification of the underlying process. For example, if drag reduction is dependent on white water, foam and spray production, we may speculate that in a hurricane those processes will be dependent upon larger scale wave and wind field properties and, therefore, may depend on factors other than absolute local wind speed. For example, Ulhorn and Black (2003) find that the algorithm used to estimate wind speed from the airborne SFMR, an instrument that remotely senses passive microwave radiation in a spectral region most sensitive to white water, appears to be different in different quadrants of a hurricane. Nevertheless, the adoption of a simple cap appears to greatly improve model performance in situations of extreme wind forcing and may be used until a more physically based refinement of the atmospheric input source term is developed.

## 5. REFERENCES

Bidlot, J., Janssen, P.A.E.M., and Abdalla, S., (2005). A revised formulation for ocean wave dissipation in CY29R1, ECMWF Momorandum Research Department F60.9/JB/0516, 35pp.

Bye J. A. T. and A. D. Jenkins, 2006. Drag coefficient reduction at very high wind speeds. J. Geophys. Res., Vol. 111, C03024.

Cardone, V. J., W. J. Pierson and E. G. Ward, 1976. Hindcasting the directional sprectra of hurricane generated waves. J. Petrol. Technol. 28, 385-394.

Cardone, V. J. and D. B. Ross, 1979. State-of-the-art wave prediction methods and data requirements. Ocean Wave Climate ed. M. D. Earle and A. Malahoff. Plenum Publishing Corp., 1979, 61-91.

Cardone, V. J., C.V. Greenwood and J. A. Greenwood. 1992. Unified program for the specification of tropical cyclone boundary layer winds over surfaces of specified roughness. Contract Rep. CERC 92-1, U.S. Army Engrs. Wtrwy. Experiment Station, Vicksburg, Miss.

Cardone, V.J. and C. K. Grant (1994). "Southeast Asia meteorological and oceanographic hindcast study (SEAMOS)". OSEA 94132. Offshore South East Asia 10th Conference & Exhibition. Singapore, 6-9 December 6-9.

Cardone, V. J., H.C. Graber, R.E. Jensen, S. Hasselmann and M. J. Caruso. (1995). "In search of the true surface wind field in SWADE IOP-1: ocean wave modeling perspective". The Global Atmosphere and Ocean System. 3. 107-150.

Cardone, V.J., R.E. Jensen, D.T. Resio, V.R. Swail and A.T. Cox. 1996). "Evaluation of contemporary ocean wave models in rare extreme events: the "Halloween Storm' of October, 1991 and the "Storm of the Century" of March, 1993." J. Atmos. Oceanic. Technol. 13. 198-230.

Cardone, V. J., A. T. Cox, K. A. Lisaeter and D. Szabo, 2004. Hindcast of winds, wves and currents in northern Gulf of Mexico Hurricane Lili (2002). Offshore Technology Conference, 3-6 May, 2004, Houston, TX. Paper OTC 616821.

Chao, Y.Y, Alves, J.H.G.M., and Tolman, H.L., (2005). An operational system for predicting hurricane-generated wind waves in the North Atlantic ocean, Weather and Forecasting, 20, 652-671.

Cooper, C. and J. Stear, 2005: Hurricane Climate in the Gulf of Mexico. Offshore Technology Conference paper 18416, Houston TX.

Cox, A.T., J.A. Greenwood, V.J. Cardone and V.R. Swail. (1995). "An interactive objective kinematic analysis system." The International Workshop on Wave Hindcasting and Forecasting. Banff, Alberta, 16-20 October. 109-118. (Available from Atmospheric Environment Service, Downsview, Ontario.)

Cox, A.T. and V.J. Cardone. Operational System for the Prediction of Tropical Cyclone Generated Winds and Waves. 6th International Workshop on Wave Hindcasting and Forecasting November 6-10, 2000, Monterey, California.

Cox, A.T., and V.R. Swail, 2001. A global wave hindcast over the period 1958-1997: validation and climate assessment. J. of Geophys. Res.

Cox, A. T., V. J. Cardone and F. Counillon, 2005. . Hindcast study of winds, waves and currents in northern Gulf of Mexico Hurricane Ivan (2004). Offshore Technology Conference, 2-6 May, 2005, Houston, TX. Paper OTC 17736.

Donelan, M.A., B. K. Haus, N. Reul, W. J. Plant, M. Stiassnie, H. C. Graber, O.B. Brown and E.S. Saltzman, 2004. On the limiting aerodynamic roughness of the ocean in very strong winds. Gephys. Res. Lttrs.,Vol. 31, L18306.

Forristall, G.Z., R. C. Hamilton and V. J. Cardone, 1977. Continental shelf currents in tropical storm Delia: observations and theory. J. of Phys. Oceanog. 7, 532-546.

Forristall, G. Z., E. G. Ward, V. J. Cardone, and L. E. Borgman. 1978. The directional spectra and kinematics of surface waves in Tropical Storm Delia. J. of Phys.

Forristall, G. Z., 1980. A two-layer model for hurricane driven currents on an irregular grid. J. Phys. Oceanog., 10, 9, 1417-1438.

Forristall, G.Z. and J. A. Greenwood, 1998. Directional spreading of measured and hindcasted wave spectra. Proc. 5th International Workshop on Wave Hindcasting and Forecasting, Melbourne, FL, January 26-30, 1998.

Gilhousen, D. B., 2006. A complete explanation of why moored buoy winds are less than ship winds. Mariners Weather Log, 50, 1(April), 4-7.

Graber, H.C., V.J. Cardone, R.E. Jensen, D.N. Slinn, S.C. Hagen, A.T. Cox, M.D. Powell, and C. Grassl, 2006 : "Coastal forecasts and storm surge predictions for tropical cyclones: A timely partnership program.", Oceanography,vol. 19 no. 1, pp.130-141

Graham , H. E. and G. N. Hudson, 1960. Surface winds near the center of hurricanes (and other cyclones).National Hurricane Research Project Report No. 39. Washington, D.C. 200 pp.

Greenwood, J.A., V.J. Cardone and L. M. Lawson, 1985. Intercomparison test version of the SAIL wave model. Oean Wave Modelling, the SWAMPO Group, Plenum Press, 221-233.

Gunther, H.P.L. and 14 coauthors. (1992). "Implementation of a third generation ocean wave model at the European Center for Medium Range Weather Forecasts." ECMWF Tech. Rep. 68.. European Center for Medium Range Weather Forecasting, Reading, United Kingdom. 34 pp.

Gunther, H., Hasselmann, S., and Janssen, P.A.E.M., (1992). Report No. 4: The WAM model cycle 4. DKRZ, 91pp.

Gunther, H., (2005). WAM cycle 4.5, Institute for Coastal Research GKSS Research Centre Geesthacht, 40pp.

Hasselmann, S and Hasselmann, K.,1981. A symmetrical method of computing the non-linear transfer in a gravity wave spectrum. Hamb. Geophys. Einzelschriften, Reihe A: Wiss. Abhand, 52, 138pp.

Hersbach, H. and Janssen, P.A.E.M., (1999). Improvement of the short-fetch behavior in the Wave Ocean Model (WAM)., J. Phys. Oceanogr. 16, 884-892.

Holland, G. J., 1980. An analytical model of the wind and pressure profiles in hurricanes. Mon. Wea. Rev. 1980, 108, 1212-1218.

Janssen, P.A.E.M.. (1991). "Quasi-linear theory of wind-wave generation applied to wave forecasting." J. Phys. Oceanog.. 2. 1631-1642.

Janssen, P.A.E.M., B. Hansen, and J. Bidlot, 1997. Verification of ECMWF wave forecasting systems against buoy and altimeter data. To appear in Weather and Forecasting ( December).

Khandekar, M.L., R. Lalbeharry and V.J. Cardone (1994). "The performance of the Canadian spectral ocean wave model (CSOWM) during the Grand Banks ERS-1 SAR wave spectra validation experiment." Atmosphere-Ocean. 32. 31-60.

Komen G. J., L. Cavalieri, M. Donelan, K. Hasselmann, S. Hasselmann and P.A.E.M. Janssen. (1994). "Dynamics and Modeling of Ocean Waves". Cambridge University Press. 532pp.

Leverette, S., S. Bian, D. Taberner and C. Van-der-Linden, 2005. Matterhorn SeaStar Hurricane Ivan response. Deep Ocean Technology, Brazil, November, 2005.

Moon, I-J, Ginnis, I., and Hara, T., (2004). Effect of surface waves on air-sea momentum exchange, part II: behavior of drag coefficient under tropical cyclones, J . Atmospheric. Sciences, 61, 233-2348.

Powell, M. D., S. H. Houston, L. R. Amat, and N Morisseau-Leroy, 1998: The HRD real-time hurricane wind analysis system. J. Wind Engineer. and Indust. Aerodyn. 77&78, 53-64

Powell, M.D., Vickery, P.J., and Reinhold, T.A., 2003: Reduced drag coefficient for high wind speeds in tropical cyclones, Nature, Vol 422, 279-283.

Ross, D. B. and V. J. Cardone, 1978. A comparison of parametric and spectral hurricane wave prediction products. Turbulent Fluxes through the Sea Surface, Wave Dynamics, and Prediction, A. Favre and K. Hasselmann, editors, 647-665.

Snyder, R.L., Dobson, F.W., Elliott, J.AS., and Long, R.L. (1981). Array measurements of atmospheric pressure fluctuations above surface gravity waves. J. Fluid Mech., 102, 1-59.

Swail, V.R. and A.T. Cox, 2000. On the use of NCEP/NCAR reanalysis surface marine wind fields for a long term North Atlantic wave hindcast. J. Atmos. Ocean. Technol., 17, 532-545..

Swail, V.R., V.J. Cardone, M. Ferguson, D.J. Gummer, E.L. Harris, E.A. Orelup and A.T. Cox, 2006 The MSC50 Wind and Wave Reanalysis. 9th International Wind and Wave Workshop, September 25-29, 2006, Victoria, B.C.

Thompson, E. F. and V. J. Cardone. 1996. Practical modeling of hurricane surface wind fields. ASCE J. of Waterway, Port,Coastal and Ocean Engineering. 122, 4, 195-205

Tolman, H., (2002). Alleviating the garden sprinkler effect in wind wave models. Ocean Modell., 4, 269-289.

Tolman, H.L., Alves, J.H.G.M., and Chao, Y.Y., (2005) Operational forecasting of wind-generated waves by Hurricane Isabel at NCEP, Wea. Forecasting, 20, 544-557.

The SWAMP Group (1985). Sea wave modeling project (Sea WAve Modeling Project), an intercomparison study of wind wave predictions models, part 1: Principal results and conclusions, in Ocean wave modeling, Plenum, New York, 256pp.

Ulhorn, E. W. and P. G. Black , 2003. Verification of remotely sensed sea surface winds in hurricanes. J. Atmos.Oceanic Technol., 20, 99-116.

Von Ahn, J. Sienkiewicz and P. S. Chang, 2006. Operational impact of QuikSCAT winds at the NOAA Ocean Prediction Center. Wea. and Forecasting., Vol. 21, 4, 523-539.

WAMDIG, (1988). The WAM model – a third generation ocean wave prediction model. J. Phys. Oceanogr., 18, 1775-1810.

Wright, C.W., Walsh, E.J., Vandermark, D., Krabill, W.B., Garcia, A.W., Houston, S.H., Powell, M.D., Black P.G., and Marks, F.D., (2001). Hurricane directional wave spectrum spatial variation in the open ocean, J. Phys. Oceanogr. 31, 2437-2488.

Wu, J., 1982. Wind-stress coefficients over the sea surface from breeze to hurricane. J. Geophys. Res., 87, 9704-9706.
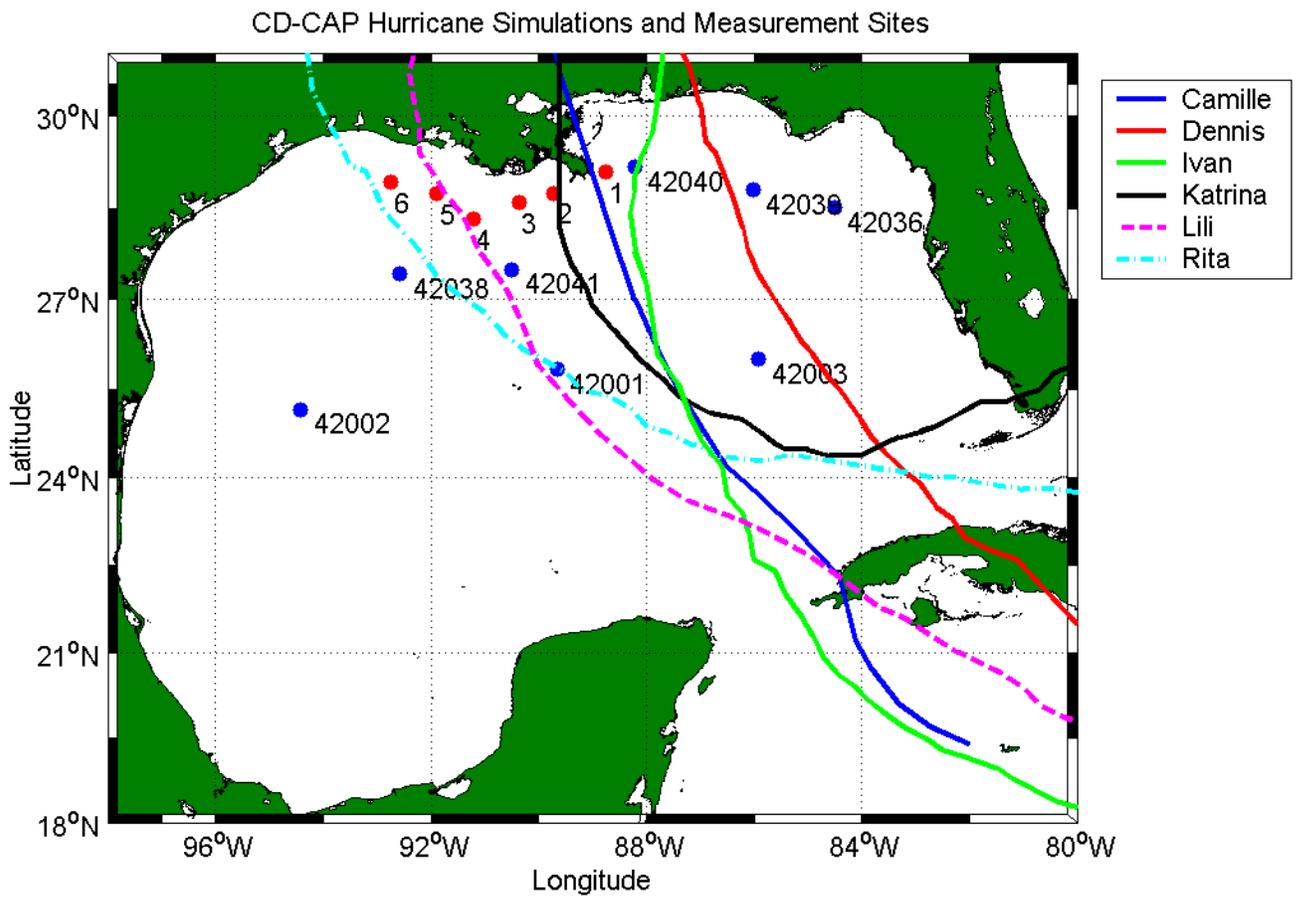
Figure 1. Tracks of hurricane hindcast with NDBC and ODGP wave measurement sites.
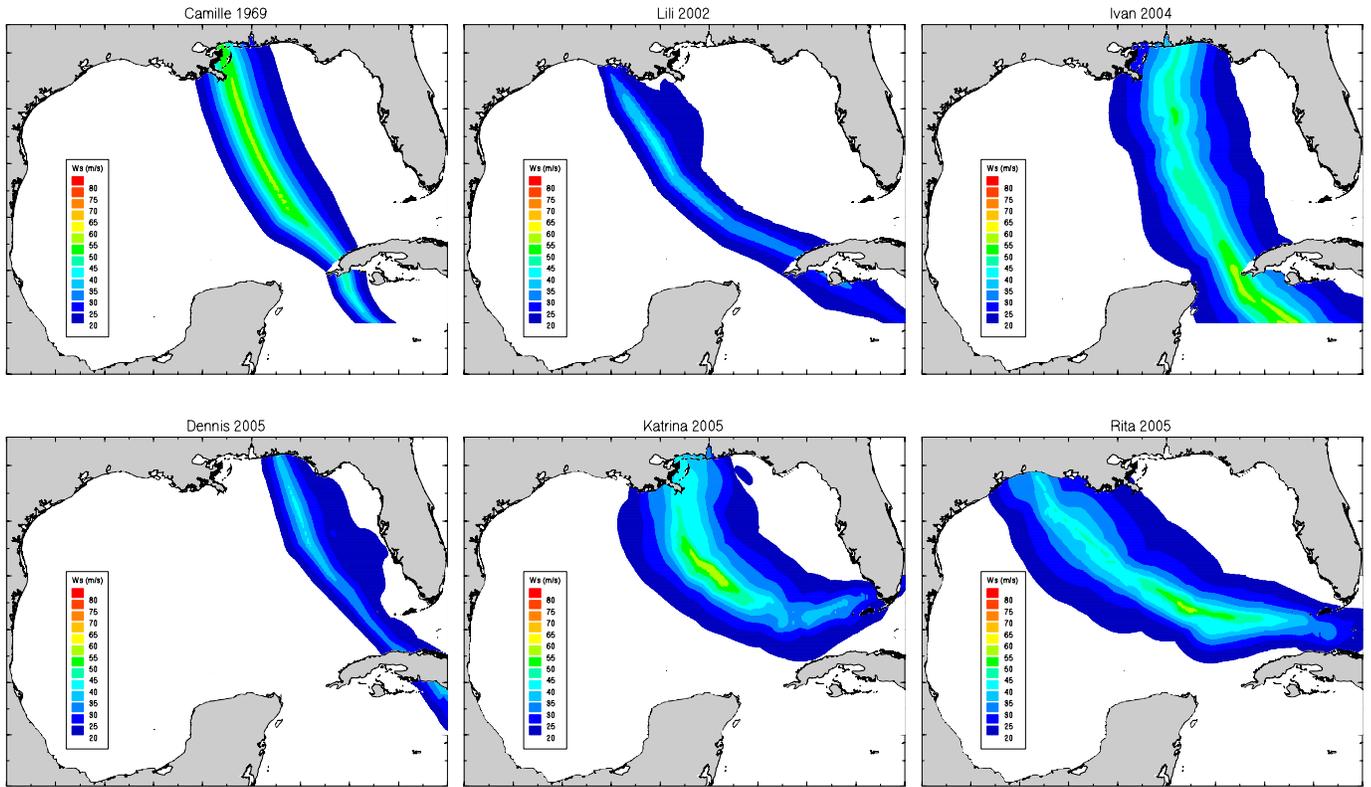
Figure 2. Comparison of envelope of maximum hindcast wind fields in six hurricanes.
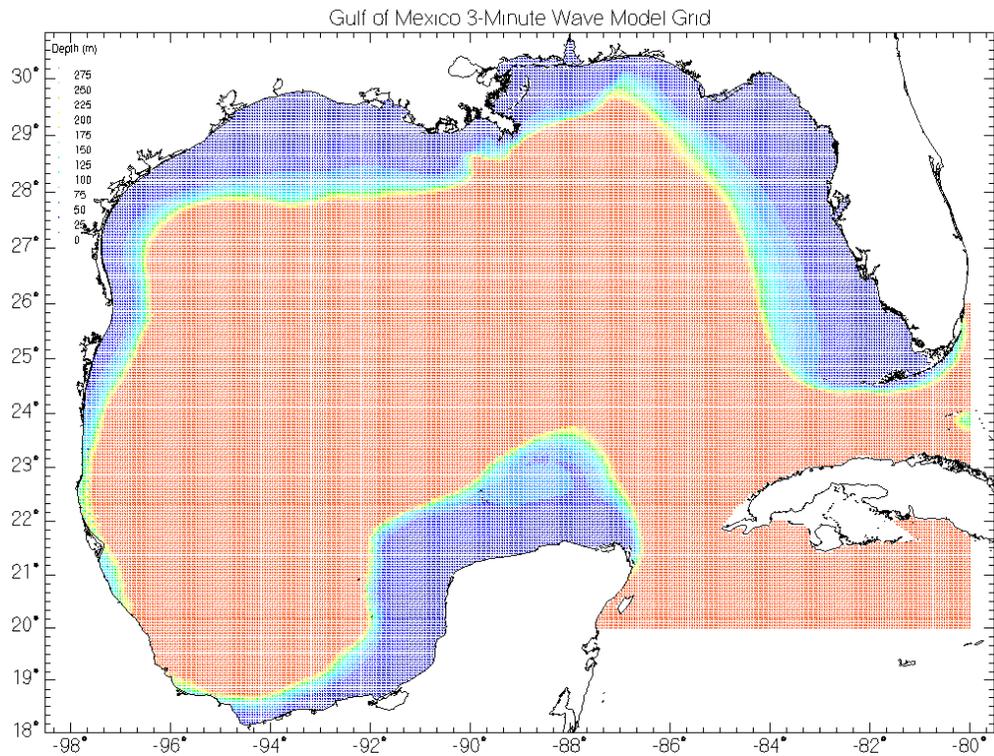


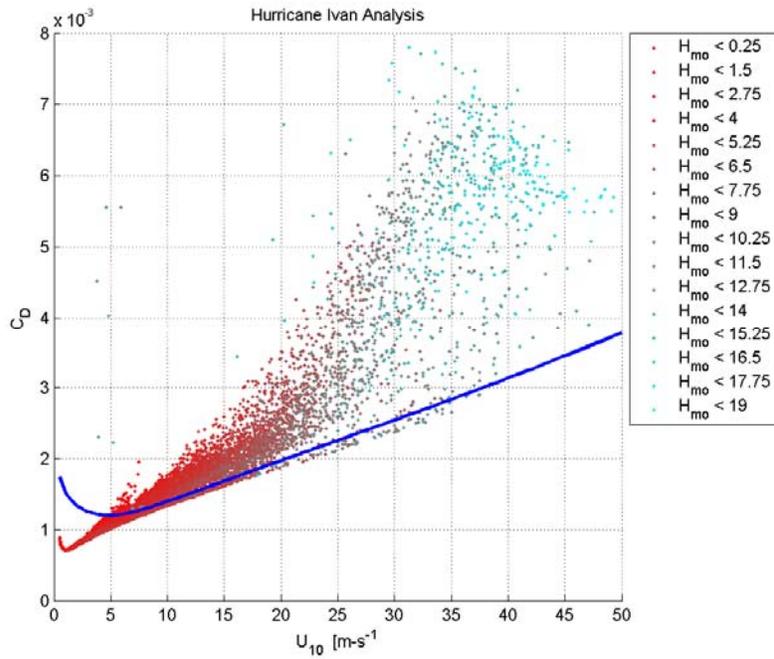Figure 3. 3-Minute wind and wave hindcast model grid.

Figure 4. Distribution of 10-meter drag coefficient implied by Janssen et al. (1991) algorithm within Hurricane Ivan for nominal WAM 4.5 model.
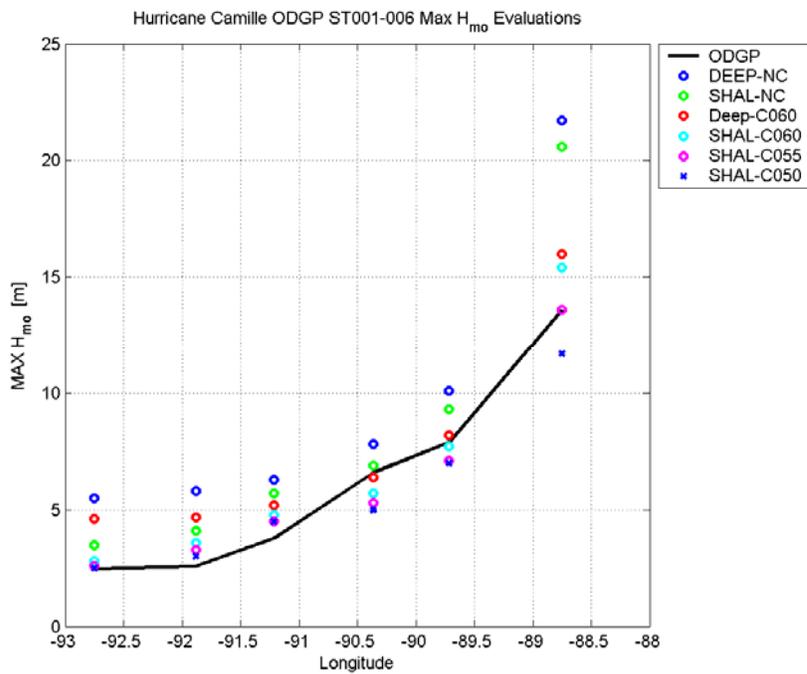


Figure 5. Comparison of measured Hmo at Camille ODGP measurement stations vs. WAM variants.
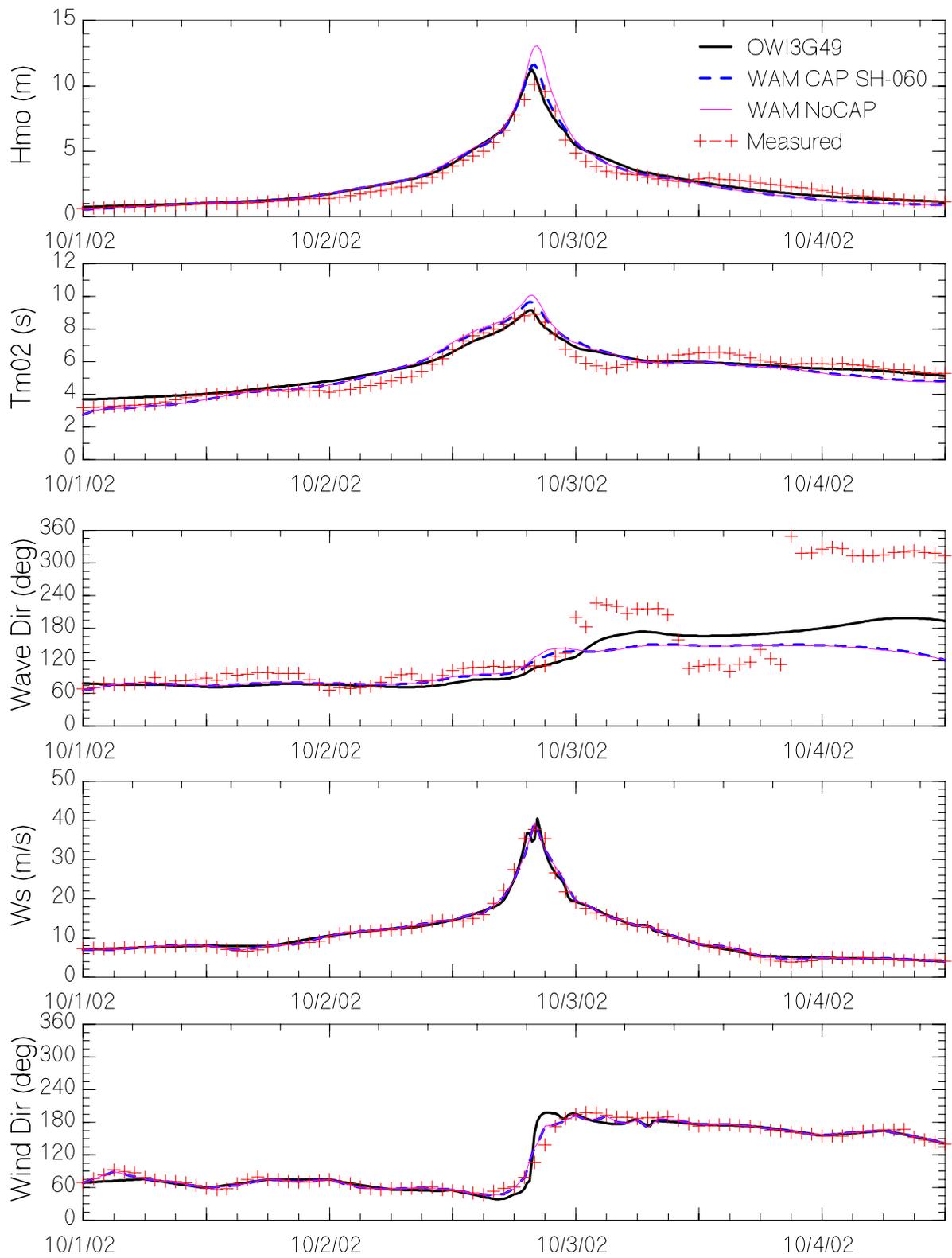
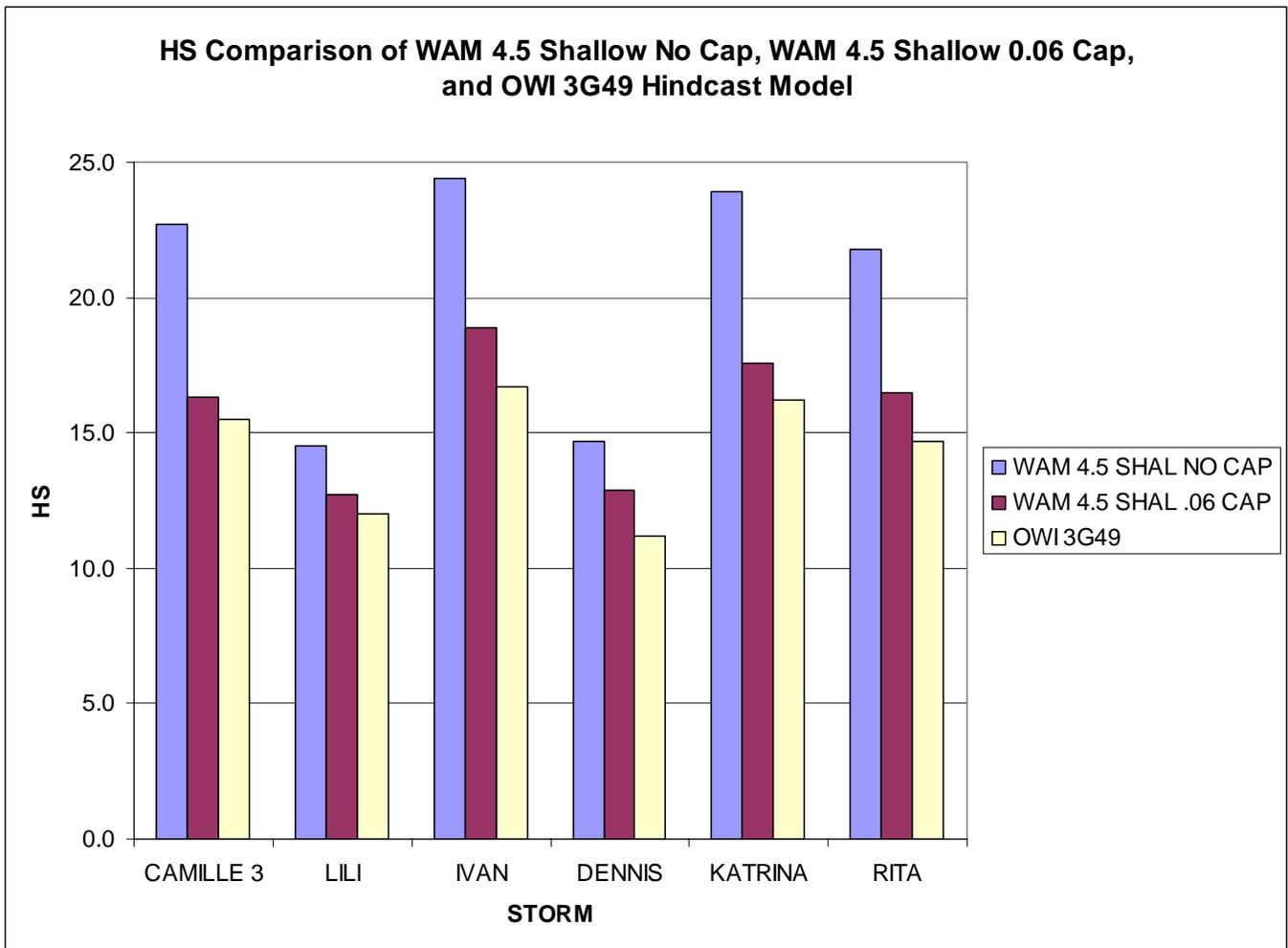Figure 6. Timeseries comparison at NDBC Buoy 42001 during Hurricane Lili.

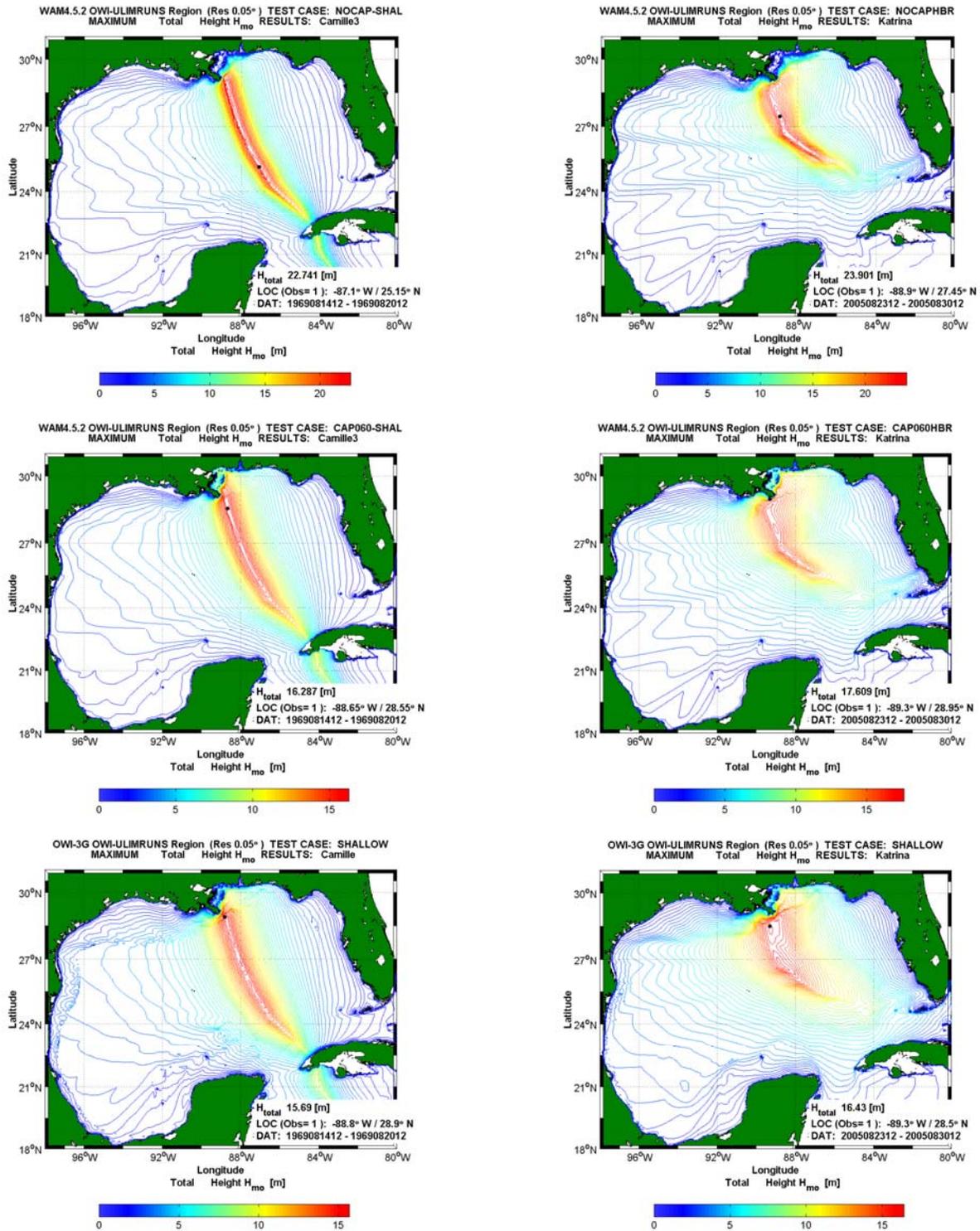Figure 7. Comparison of maximum hindcast Hmo during six storms.

Figure 8 Peak Hmo hindcast in Camille (left) Katrina (right) using WAM NoCAP (top), WAM CAP (middle) and OWI3G (bottom).
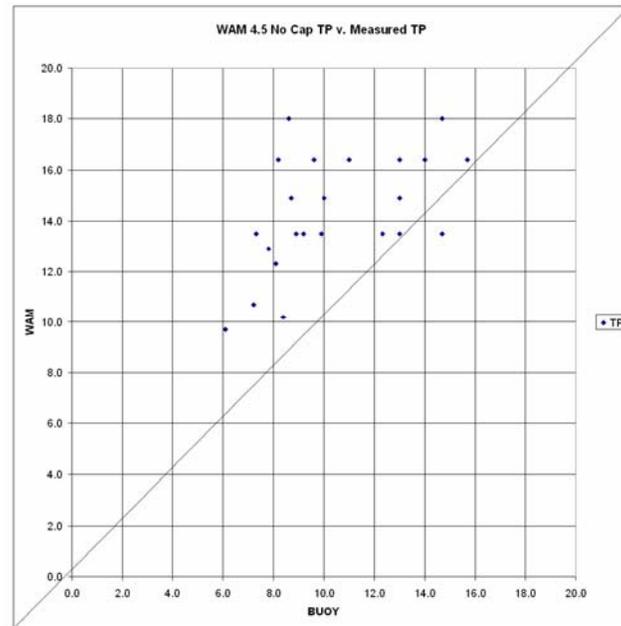
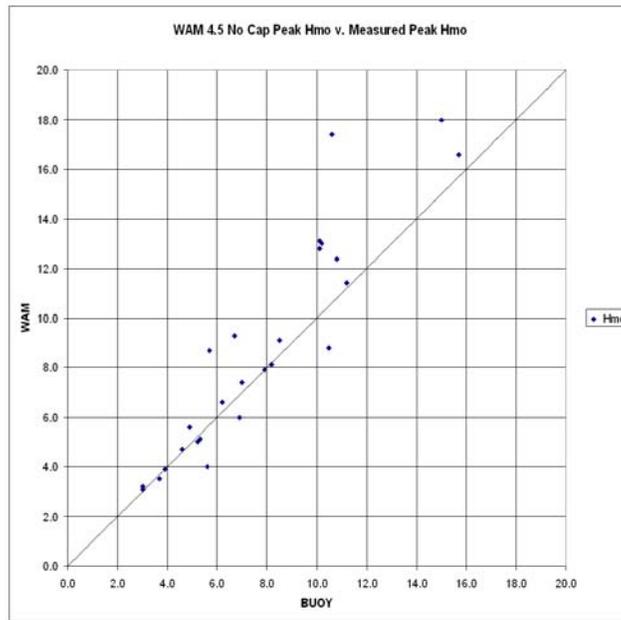Figure 9. Comparison of measured peak Hmo (top) and associated peak wave period (below) for combined NDBC buoys vs. WAM 4.5 (No Cap).
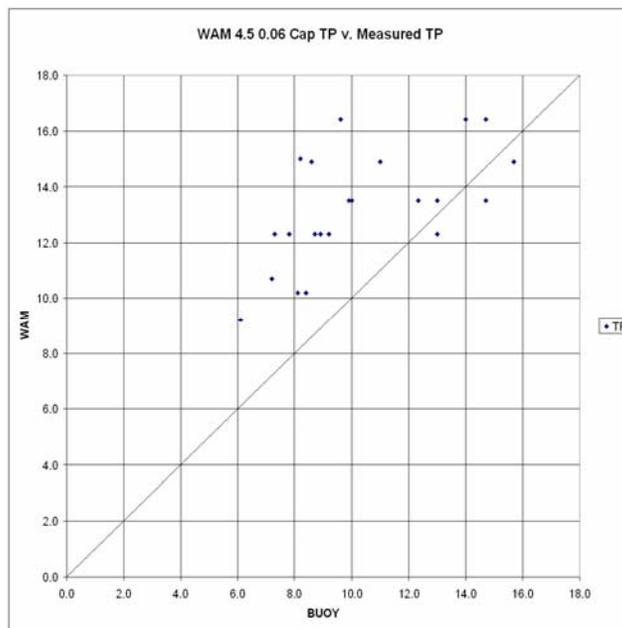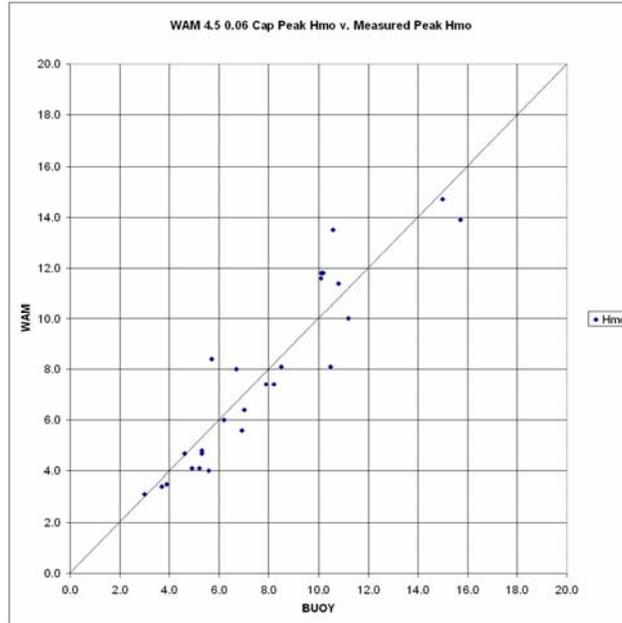
Figure 10. Comparison of measured peak Hmo (top) and associated peak wave period (below) for combined NDBC buoys vs. WAM 4.5 (0.06 Cap).
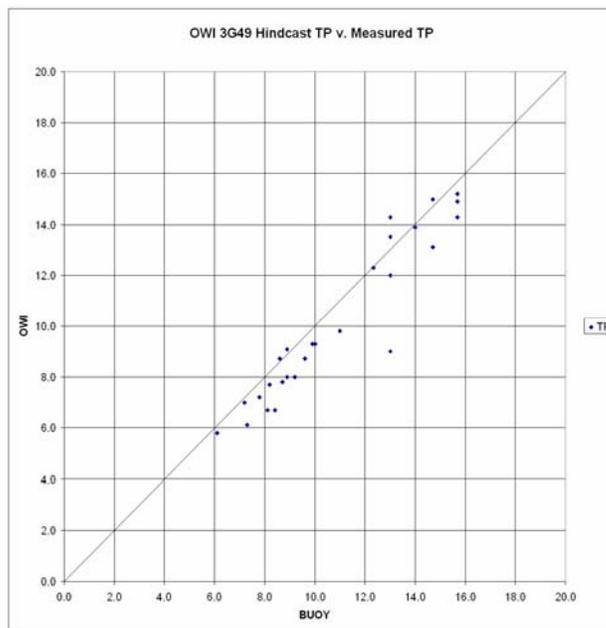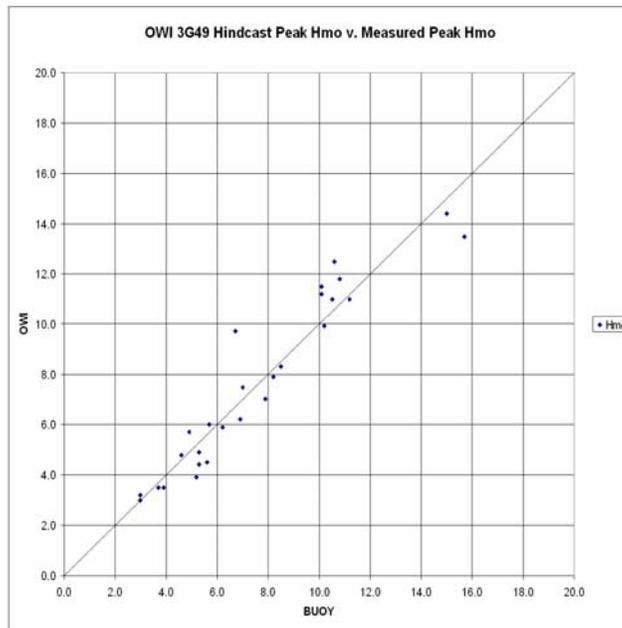
Figure 11. Comparison of measured peak Hmo (top) and associated peak wave period (below) for combined NDBC buoys vs. OWI3G49.

Table 1. Absolute hindcast storm peaks (Hmo in meters).

| TYPE | STORM | Hmo | Lat | Lon |
|---|---|---|---|---|
| WAM 4.5 SHAL NO CAP | CAMILLE 3 | 22.7 | 25.15 | -87.10 |
| WAM 4.5 SHAL NO CAP | LILI | 14.5 | 27.05 | -90.40 |
| WAM 4.5 SHAL NO CAP | IVAN | 24.4 | 28.10 | -87.80 |
| WAM 4.5 SHAL NO CAP | DENNIS | 14.7 | 28.60 | -86.20 |
| WAM 4.5 SHAL NO CAP | KATRINA | 23.9 | 27.45 | -89.90 |
| WAM 4.5 SHAL NO CAP | RITA | 21.8 | 27.75 | -91.80 |
| WAM 4.5 SHAL .06 CAP | CAMILLE 3 | 16.3 | 28.55 | -88.65 |
| WAM 4.5 SHAL .06 CAP | LILI | 12.7 | 27.05 | -90.40 |
| WAM 4.5 SHAL .06 CAP | IVAN | 18.9 | 28.20 | -87.85 |
| WAM 4.5 SHAL .06 CAP | DENNIS | 12.9 | 28.55 | -86.20 |
| WAM 4.5 SHAL .06 CAP | KATRINA | 17.6 | 28.95 | -89.30 |
| WAM 4.5 SHAL .06 CAP | RITA | 16.5 | 27.75 | -91.80 |
| OWI 3G49 | CAMILLE 3 | 15.5 | 27.90 | -88.40 |
| OWI 3G49 | LILI | 12.0 | 27.05 | -90.40 |
| OWI 3G49 | IVAN | 16.7 | 20.00 | -83.25 |
| OWI 3G49 | DENNIS | 11.2 | 27.00 | -85.55 |
| OWI 3G49 | KATRINA | 16.2 | 26.85 | -88.80 |
| OWI 3G49 | RITA | 14.7 | 24.55 | -86.35 |

Table 2. Hindcast and buoy peak Hmo abd associated Tp in 21st century hurricanes (Hmo in meters, To in seconds).

| STORM | STATION | WAM 4.5 SHAL NO CAP Hmo | TP | DDHH | WAM 4.5 SHAL .06 CAP Hmo | TP | DDHH | OWI 3G49 Hmo | TP | DDHH | SITE BUOY Hmo | TP | DDHH |
|---|---|---|---|---|---|---|---|---|---|---|---|---|---|
| LILI | 42001 | 13.1 | 13.5 | 030500 | 11.6 | 12.3 | 022000 | 11.2 | 9.1 | 021900 | 10.1 | 8.9 | 022000 |
| | 42002 | 3.5 | 13.5 | 020500 | 3.4 | 12.3 | 030630 | 3.5 | 8.0 | 030700 | 3.7 | 9.2 | 030500 |
| | 42003 | 4.0 | 10.2 | 021245 | 4.0 | 10.2 | 021245 | 4.5 | 6.7 | 021000 | 5.6 | 8.4 | 020900 |
| | 42039 | 3.1 | 9.7 | 021930 | 3.1 | 9.2 | 022000 | 3.0 | 5.8 | 022130 | 3.0 | 6.1 | 021900 |
| | 42040 | 4.7 | 10.7 | 030615 | 4.7 | 10.7 | 030645 | 4.8 | 7.0 | 030730 | 4.6 | 7.2 | 030700 |
| | 42041 | 12.8 | 13.5 | 030200 | 11.8 | 13.5 | 030200 | 11.5 | 9.3 | 030245 | 10.1 | 9.9 | 030200 |
| IVAN | 42001 | 9.1 | 16.4 | 150503 | 8.1 | 14.9 | 150615 | 8.3 | 14.3 | 150900 | 8.5 | 15.7 | 150600 |
| | 42002 | 5.0 | 16.4 | 151045 | 4.1 | 14.9 | 151145 | 3.9 | 15.2 | 151100 | 5.2 | 15.7 | 151400 |
| | 42003 | 12.4 | 14.9 | 151115 | 11.4 | 13.5 | 151115 | 11.8 | 14.3 | 150300 | 10.8 | 13.0 | 150200 |
| | 42036 | 6.6 | 16.4 | 151530 | 6.0 | 13.5 | 151500 | 5.9 | 13.5 | 151400 | 6.2 | 13.0 | 152000 |
| | 42039 | 11.4 | 16.4 | 152145 | 10.0 | 16.4 | 152315 | 11.0 | 13.9 | 160200 | 11.2 | 14.0 | 152100 |
| | 42040 | 18.0 | 18.0 | 152345 | 14.7 | 16.4 | 152315 | 14.4 | 15.0 | 152300 | 15.0 | 14.7 | 152300 |
| | 42041 | 8.1 | 16.4 | 151230 | 7.4 | 14.9 | 151400 | 7.9 | 14.9 | 151700 | 8.2 | 15.7 | 151300 |
| DENNIS | 42003 | 8.7 | 13.5 | 100500 | 8.4 | 12.3 | 100500 | 6.0 | 12.0 | 100100 | 5.7 | 13.0 | 092300 |
| | 42038 | 3.2 | 13.5 | 102100 | 3.1 | 13.5 | 102115 | 3.2 | 13.1 | 102100 | 3.0 | 14.7 | 110100 |
| | 42039 | 13.0 | 13.5 | 101245 | 11.8 | 13.5 | 101230 | 9.9 | 12.3 | 101300 | 10.2 | 12.3 | 101400 |
| KATRINA | 42001 | 9.3 | 18.0 | 281445 | 8.0 | 14.9 | 281715 | 9.7 | 8.7 | 281800 | 6.7 | 8.6 | 281700 |
| | 42003 | 8.8 | 14.9 | 290545 | 8.1 | 13.5 | 280530 | 11.0 | 9.0 | 280400 | 10.5 | 13.0 | 280600 |
| | 42036 | 5.1 | 12.3 | 291230 | 4.8 | 10.2 | 291330 | 4.4 | 6.7 | 281900 | 5.3 | 8.1 | 291000 |
| | 42038 | 7.4 | 16.4 | 290345 | 6.4 | 16.4 | 290400 | 7.5 | 8.7 | 290300 | 7.0 | 9.6 | 290200 |
| | 42039 | 7.9 | 13.5 | 290900 | 7.4 | 12.3 | 291215 | 7.0 | 8.0 | 282200 | 7.9 | 8.9 | 291300 |
| | 42040 | 16.6 | 16.4 | 291045 | 13.9 | 14.9 | 291045 | 13.5 | 9.8 | 291100 | 15.7 | 11.0 | 291200 |
| RITA | 42001 | 17.4 | 14.9 | 222100 | 13.5 | 13.5 | 222045 | 12.5 | 9.3 | 222000 | 10.6 | 10.0 | 222000 |
| | 42002 | 5.6 | 16.4 | 230345 | 4.1 | 15.0 | 230415 | 5.7 | 7.7 | 231400 | 4.9 | 8.2 | 231300 |
| | 42036 | 3.9 | 13.5 | 220915 | 3.5 | 12.3 | 231500 | 3.5 | 6.1 | 230400 | 3.9 | 7.3 | 230400 |
| | 42039 | 5.1 | 12.9 | 222015 | 4.7 | 12.3 | 221945 | 4.9 | 7.2 | 222000 | 5.3 | 7.8 | 222000 |
| | 42040 | 6.0 | 14.9 | 222230 | 5.6 | 12.3 | 230445 | 6.2 | 7.8 | 231400 | 6.9 | 8.7 | 230700 |

Table 3. Comparison of hindcast and buoy peaks Hmo and associated Tp for validated hurricanes.

| | HS | | | | TP | | | |
|---|---|---|---|---|---|---|---|---|
| | BIAS | STD DEV. | SCATTER INDEX | CC | BIAS | STD DEV. | SCATTER INDEX | CC |
| WAM 4.5 Shallow  No Cap | 0.89 | 1.81 | 0.24 | 0.93 | 3.62 | 2.50 | 0.23 | 0.57 |
| WAM 4.5 Shallow 0.06 Cap | -0.08 | 1.81 | 0.17 | 0.93 | 2.45 | 2.34 | 0.22 | 0.62 |
| OWI  3G49 | 0.03 | 1.06 | 0.14 | 0.95 | -0.72 | 0.96 | 0.09 | 0.95 |